Universiteit
Leiden
The Netherlands

Probing spatial heterogeneity in supercooled glycerol and temporal heterogeneity with single-molecule FRET in polyprolines

Xia, T.

Citation
Xia, T. (2010, March 25). *Probing spatial heterogeneity in supercooled glycerol and temporal heterogeneity with single-molecule FRET in polyprolines*. *Casimir PhD Series*. Retrieved from https://hdl.handle.net/1887/15122

Version:	Corrected Publisher's Version
License:	Licence agreement concerning inclusion of doctoral thesis in the Institutional Repository of the University of Leiden
Downloaded from:	https://hdl.handle.net/1887/15122

Note: To cite this publication please use the final published version (if applicable).

6 Temperature-cycle microscopy of single-molecule FRET in polyprolines

Abstract –We investigate the conformational dynamics of polyprolines by single-molecule Förster resonance energy transfer (FRET) combined with a temperature-cycle microscopic technique developed in our group. We first measure the static FRET efficiency of individual frozen constructs in a thin glycerol film at a low temperature. The measurements on polyproline 6 and polyproline 20 reveal a broad FRET distribution. The broadening stems from the wide distribution of the orientation factor and the fluctuation of the interdye distance. In the fluorescence time traces of the individual constructs, we study variation of the donor and acceptor signals and observe 3 types of events. (1) A correlation between the two signals, i.e., the acceptor intensity is positively correlated with the donor intensity, is observed when the donor is in a dark state or bleached. (2) A noncorrelation, i.e., the acceptor intensity changes independently of the donor intensity, is seen when the acceptor is in non-fluorescing states and it could still accept the excitation energy from the donor. (3) An anticorrelation between the donor and acceptor intensity is detected if a non-fluorescing form of the acceptor is not able to quench the donor emission. We performed our first temperature-cycle measurements on polyproline 6 molecules and we could indeed detect the conformational changes induced by temperature jumps by measuring the FRET efficiency. These preliminary results demonstrate that temperature-cycle microscopy combined with single-molecule FRET has potential for studies of protein-folding dynamics at the single-molecule level.

6.1 Introduction

The study of single molecules in biological systems has been booming in the last decade. Because single-molecule techniques are intrinsically free from ensemble averaging, they are particularly appealing in addressing biological processes in which heterogeneity is native to the structure or dynamics of the systems, such as enzymatic reactions, protein-DNA or -RNA interactions, and protein-folding. Single-molecule techniques can be divided into two categories in general. One category gathers force-based approaches, which typically involve an atomic force microscope (AFM), or optical/magnetic tweezers, and allow to study mechanical properties of single biomolecules, like DNA molecules [108–111] and proteins [112–114], or interactions between biomolecules, such as protein-DNA interactions, e.g., in nucleosomes [115,116] and chromatin [117,118]. The other class is based on single-molecule optical detection, which requires microscopes to detect optical signals by absorption, emission (fluorescence), scattering, or a combination of these using labeled systems. The information from the detected optical signals has to be related to the underlying molecular process. These two approaches provide molecular information about different aspects and thus are complementary. If they are employed in the same experiment, one will uncover more details about biological processes under investigation than with either of them alone. This will further extend the capability of single-molecule methods to address more complicated processes, e.g., the transcriptional machinery. Indeed, several groups have demonstrated the feasibility of combining force measurements with fluorescence to study protein-DNA interactions in vitro [119–122].
Among the optical-based methods, single-molecule fluorescence spectroscopy has been widely used in biological applications because of its high sensitivity, selectivity and versatility [123–125]. A single dye-labeling typically allows to probe translational and/or rotational diffusion of individual labeled biomolecules and thus to gain the information on their mobility in certain environments. This has been used, for instance, to study the mobility of cAMP-receptor on the plasma membrane of chemotacting cells in directional sensing [126]. Labeling with two different dyes enables to study inter- or intramolecular interactions on the length scale of $10 - 75\,\text{Å}$ by Förster resonance energy transfer (FRET), [33, 34]. The length scale is about one to two orders of magnitude smaller than the wavelength of visible light. The FRET technique thus proves to be a powerful "spectroscopic ruler". Since the first demonstration of single-molecule FRET by Ha et al. in 1996 [35], many experiments have been designed for biological applications [36–41,43,44,127]. In the FRET process, excitation energy from a donor is transferred to an acceptor

via a near-field dipole-dipole interaction. The efficiency of energy transfer, E, is given by

$$E = \frac{1}{1 + \left(\frac{R}{R_0}\right)^6} \quad ,$$

where R is the distance between the donor and acceptor and R_0 is the Förster radius, at which 50 % of the energy is transferred. It is a function of the properties of the dyes. The distance R_0 (in Å) is calculated in the Förster theory according to the following equation [128]:

$$R_0 = 9.78 \times 10^3 (\kappa^2 n^{-4} \phi_D J(\lambda))^{1/6} \quad ,$$

$$J(\lambda) = \int_0^\infty F_D(\lambda) \epsilon_A(\lambda) \lambda^4 d\lambda \quad ,$$

where $J(\lambda)$ is the normalized overlap integral between the donor emission, $F_D(\lambda)$, and the acceptor absorption, $\epsilon_A(\lambda)$. ϕ_D is the donor's fluorescence quantum yield and n is the refractive index of the medium between the dyes. The factor κ^2 is depends on the relative orientation between the two dyes and can vary from 0 to 4. If the dipole moments of donor and acceptor are free to rotate isotropically on a time scale much faster than their radiative lifetimes, a geometric averaging of all the angles will result in a value of 2/3 for κ^2. The FRET efficiency, E, determined through the fluorescence intensities from both the donor and acceptor or the fluorescence lifetimes of the donor in the presence and absence of the acceptor, can then be related to the inter-dye distance, R. However, since the fluorophores may interact with the host molecule to which they are attached and this interaction will restrict their motion, the averaged angular factor may differ from 2/3 and should be checked carefully for the proper calculation of R.

When performing single-molecule FRET experiments on biological systems, one can detect dual-labeled molecules in two different ways. One way is to detect freely diffusing molecules in a solution with a confocal microscope. When the molecule diffuses through the confocal volume, a photon burst from the labels can be detected. The FRET efficiency from each burst is calculated and the associated histogram can be constructed. In addition, fast dynamics on the time scale of microseconds can be probed by performing Fluorescence Correlation Spectroscopy (FCS). The detection of freely diffusing molecules is relatively easy to perform and there are no complications resulting from immobilization procedures. However, as the molecules only reside in the detection volume for a limited time period, the slow dynamics on time scales much larger

than the characteristic diffusion time of the molecules are not accessible. To probe such slow dynamics, one normally immobilizes the molecules on a surface. The molecule can be attached directly through a linker or encapsulated within a surface tethered vesicle [129]. Individual molecules can then be studied one at a time via a confocal configuration or in parallel via a wide-field imaging setup. Although immobilization enables to access slow dynamics, in practice it often involves sophisticated surface preparations and tethering chemistries, which sometimes can introduce artifacts into the dynamics or affect the structure of the molecules of interest. In addition, since the molecule is illuminated all the time during the measurements, one limiting factor is the photophysical behavior of the dyes, namely, photoblinking and photobleaching. Photoblinking is the reversible transition of a fluorophore between a fluorescing state and a non-fluorescing state, a "dark" state, which is induced by the excitation light [45] and can sometimes complicate the interpretation of the FRET results [44]. Photobleaching is the irreversible conversion of a fluorescent molecule into a non-fluorescent entity, which limits the observation time of the molecules. Moreover, since a single dye molecule can only emit a limited number of photons per second, a certain minimum integration time has to be chosen in order to obtain a reasonable signal-to-noise ratio, which restricts the accessible dynamics on the short times. The above mentioned limitations are generic in room-temperature single-molecule fluorescence measurements.

To achieve longer observation windows and access fast dynamics from single-molecules, our group has developed a new type of temperature-cycle microscopy [46]. The method relies on (a) rapid freeze-thaw cycle(s) of a microscopic sample to separate the conformational evolution of a single molecule at room-temperature from the optical probing of the fluorescent label(s), which takes place at low temperature where the photophysical parameters of the label(s) are more favorable than at room-temperature. The temporal resolution in this case is only determined by the time it takes to undergo the temperature jump, which has been shown to be as short as a few microseconds [46]. This leads to an improvement in time resolution of about three orders of magnitude compared to conventional single-molecule experiments at room-temperature. In addition, the temperature at which dynamics take place and the duration of dynamics can be well controlled by tuning the heating power and heating period, respectively. The control of temperature opens the possibility of manipulating some reactions or processes in which the temperature determines the probability to pass activation barriers. Hence, temperature variation allows not only to determine the height of an activation barrier (Arrhenius law),

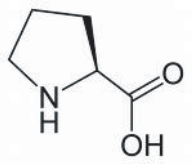

Figure 6.1: Structure of the amino acid proline.

but also to selectively block certain pathways involved in a process. These features are particularly useful to study complicated multi-pathways processes, such as protein-folding, since the associated potential-energy landscape in principle can be mapped out with our proposed temperature-cycle microscopy and thus can help to understand how a 1D polypeptide chain folds into a functional 3D structured protein.

To prove the principle of temperature-cycle microscopy, we apply this new method to the investigation of the conformational dynamics of single-molecule FRET labeled polyprolines in a thin glycerol film. Proline is one of the 20 amino acids that build up proteins. Unlike the other 19 amino acids, the side chain of proline is connected back to its backbone (see Figure 6.1), so the overall structure is considerably restricted. The oligomer of proline or polyproline can form two types of helix, a left-handed poly-Pro II helix due to the *trans* isomer of its peptide bond and a right-handed poly-Pro I helix due to the *cis* isomer. Both helices are stable and stiff. In aqueous solution polyproline usually adopts a *trans*-form poly-Pro II helix, which is energetically more favorable than a poly-Pro I helix. However, it has been shown that *cis* isomerization can take place within a poly-Pro II helix [130–132]. Since polyproline was first used as "a molecular ruler" to calibrate distances from FRET measurements by Stryer and Haugland in 1967 [34], much more effort has been devoted to characterizing its behavior in buffer solutions at room-temperature [43, 127, 131–137], providing ample reference for our low-temperature measurements on this model molecule. In our experiments, we choose glycerol as solvent for polyprolines because of the following reasons. First, glycerol is not harmful to proteins and is often added to buffer solutions in low temperature measurements to prevent ice formation during the cooling, which sometimes can disturb the structure of bio-macromolecules significantly. Second, glycerol has a very high viscosity at room-temperature, thousand times more viscous than water. Its viscosity varies by about 10 orders of magnitude from room-temperature to the glass transition (190 K) [57], and can be used to calibrate our heating for temperature-jumps [46]. In ad-

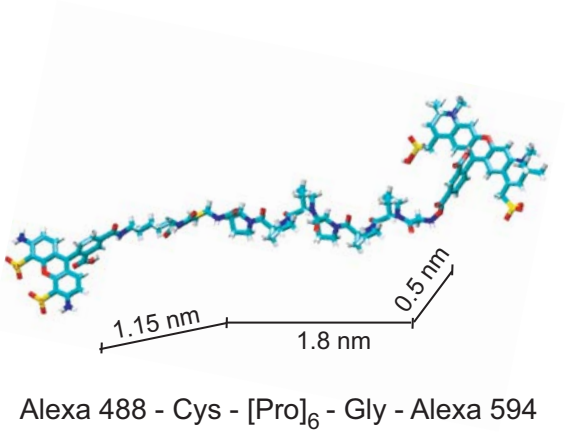

Figure 6.2: Structure of dual-labeled polyproline 6. The contour length of plyproline 6 is about 1.8 nm. The lengths of two linkers are about 1.15 nm and 0.5 nm, respectively. If the molecule is fully stretched, the interdye distance is around 3.45 nm. If the two linkers fold back to the backbone, the interdye distance is approaching to 0.15 nm.

dition, owing to its viscous nature, glycerol hardly evaporates in a dry environment, which makes the sample preparation much easier than working with normal buffer solutions. The latter typically requires a cover slip or a closed cell to prevent the sample solution from evaporating.

6.2 Experimental methods

6.2.1 Sample preparation

Alexa 488 & Alexa 594 dual-labeled and Alexa 488 single-labeled polyprolines were synthesized in the Department of Biochemistry, University of Zurich. The structure of dual-labeled polyproline 6 is shown in Figure 6.2. The labeled polyprolines were dissolved in glycerol solution at concentrations ranging from 10^{-11} to 10^{-13} M. The glycerol solution was directly spin-coated at 6000 rpm on a round glass substrate, which has a diameter of 20 mm and is coated first with a thin absorbing metal film (thickness 50 nm, Chromium) and then a layer of silica (thickness 50 nm). To improve wetting, the glass substrates were first treated in a UV-ozone cleaner (model 42-220, Jelight, Irvine, CA). The resulting thickness of the glycerol film from this procedure was $0.5-2\,\mu$m, as deduced from examination in a home-built Michelson interferometer. To

minimize the water content of glycerol, the samples were dried in the cryostat by repeatedly pumping and flushing with helium gas at room-temperature and kept under dry helium throughout all experiments.

6.2.2 Optical setup

The setup combined a low-temperature home-built confocal microscope with single-molecule sensitivity and a heating path for the fast temperature cycles. It has been described in detail in ref. [46]. The key optical components inside the cryostat are schematically shown in Figure 6.3. Briefly, the probing beam from either the 488 nm line of an Argon-ion laser (Spectra-Physics Stabilite 2017) or a 594 nm yellow HeNe laser (25LYP173-230, Melles Griot) enters the cryostat through the bottom window and is focused by a custom-made low-temperature microscope objective (NA=0.85) onto the sample. The fluorescence emitted from the sample is collected through the same objective and then spatially filtered with a 100 µm pinhole. After additional filtering to remove scattered laser (Semrock NF01-488U-25 & LP02-488RU-25 for the 488 nm laser, NF01-594U-25 for the 594 nm laser, and Thorlabs FES0700, a short-pass filter for blocking the NIR heating laser), the fluorescence is separated into donor and acceptor components by a dichroic mirror (585DCXR, AHF Analysentechnik) and three final filters (AHF Analysentechnik HQ535/50X for the donor and HQ615LP & HQ638/95M for the acceptor). Each component is focused onto a photon-counting avalanche photodiode (SPCM-AQR, Perkin-Elmer). The NIR heating beam from a 785 nm single-mode diode laser (XTRA, TOPTICA Photonics AG) enters the cryostat through one of its side windows, is directed downward by a 45° mirror and focused onto the metal film by an aspheric singlet lens (NA=0.68). The sample plate and the NIR lens (together with the 45° mirror) are separately held by a home-built cryostat insert. This insert allows us to adjust both elements in three dimensions so that the visible and NIR foci can be overlapped.
To achieve alternating illumination with probing or heating light, a mechanical shutter (VS14S2Z0-7070, UNIBLITZ) and an acousto-optical modulator (AOM) (MT100A1.5-IR, AA Opto-Electronic) were used to gate the probing (488 nm) and heating (785 nm) beam, respectively. The employed alternating-cycle is shown in Figure 6.4. A full cycle begins with the optical probing at a low temperature for a period t_1 (300 ms), then followed by a delay t_2 (100 ms) produced by the response of the mechanical shutter (10 ms). After this short break, the NIR heating laser is switched on for a very short time t_3 (10 µs) during which the temperature quickly jumps to a high temperature. At the end of the cycle another delay t_4 (100 ms) after the heating is inserted to en-

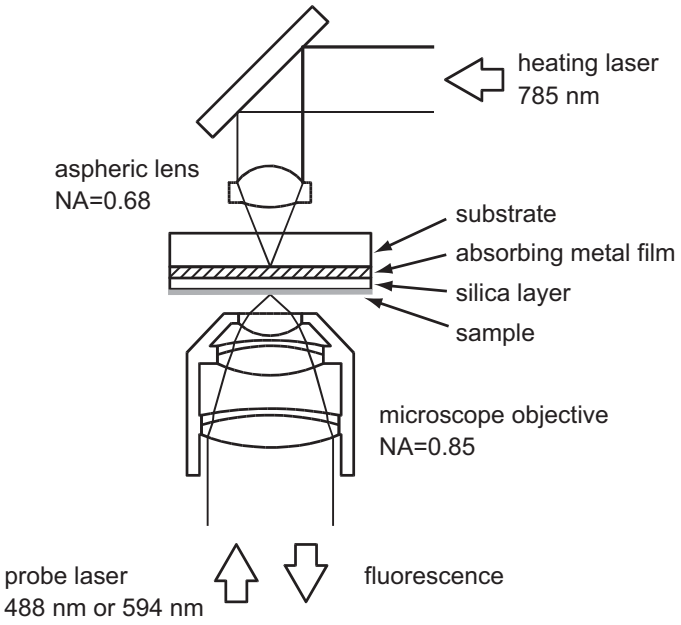

Figure 6.3: Scheme of the key optical elements around the sample plate inside the cryostat (not to scale). The figure shows the absorbing sample plate required for sufficient NIR laser absorption, which consists of a glass substrate (thickness 0.17 mm), a thin absorbing metal film (thickness 50 nm, Chromium), and a silica layer (thickness 50 nm). The fluorescent sample is spin-coated on the silica surface. Fluorescence is excited by a probe laser (488 nm or 594 nm) and collected by the custom-made ten-lens objective (NA=0.85, represented by a simplified scheme) beneath the sample. Above it, a 45° mirror and an aspheric singlet lens (NA=0.68) direct and focus the NIR heating beam (785 nm) onto the metal film above the visible focus.

sure that the temperature relaxes back to the original point before the next cycle starts. This alternating scheme was controlled by the ADwin-Gold system (Jäger Computergesteuerte Messtechnik GmbH) via our data-acquisition software written in Labview.

The confocal scanning images, $20 \times 20\,\mu m^2$ in size, were scanned with 200 by 200 pixels, a dwell time of 10 ms, and an excitation power of $2.0\,kW/cm^2$ for both 488 nm and 594 nm excitations. The fluorescence time traces were recorded with an integration time of 100 ms and an excitation power varying from 0.4 to $2.0\,kW/cm^2$.

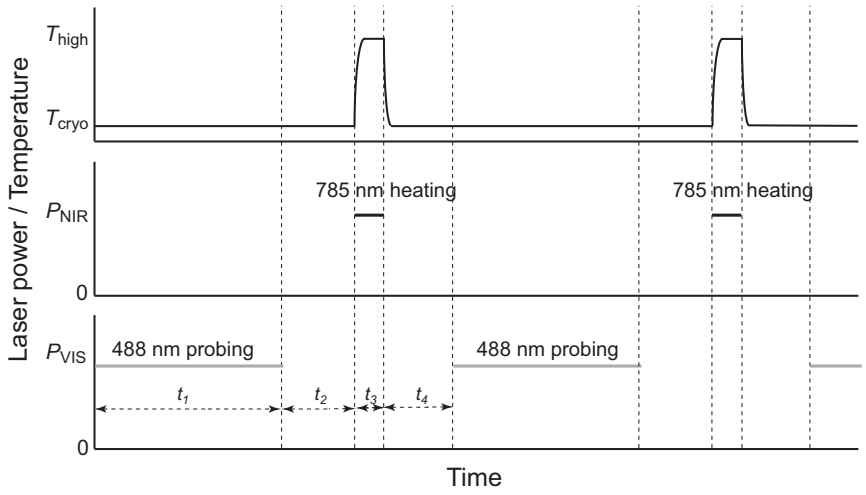

Figure 6.4: The alternating scheme of the probing and heating beams. A full cycle starts with t_1 (300 ms) during which only the probing beam is on and the fluorescence measurements take place at low temperature. Then a short delay t_2 (100 ms) follows to wait for the response of the mechanical shutter to fully block the probing beam. After this short interval, the NIR heating beam is switched on for a very short period t_3 (10 µm) during which the temperature rapidly jumps to a high temperature. Another break t_4 (100 ms) is set at the end of the cycle to allow the temperature to relax back to the initial low temperature before the new cycle begins.

6.2.3 Heating calibration

Temperature calibration of the heating spot on the metal film with the NIR laser (785 nm) was performed in the same way as described in ref. [46]. Briefly, the photoblinking of Rhodamine 6G in glycerol has a strong temperature dependence between 200 and 280 K, which gives rise to a positive sublinear relationship between the fluorescence anisotropy and the temperature. At temperatures above 280 K, the anisotropy decreases with increasing temperature according to Perrin's law [138]. The center temperature of the heating spot, therefore, can be calibrated from the fluorescence anisotropy of Rhodamine 6G (10^{-5} M) in glycerol as a function of NIR power in a series of images at varying heating power. The resulting local temperature calibration is shown in Figure 6.5 where a linear fit gives a slope of 10 K/mW, which is in good agreement with the previous calibration (10.3 K/mW) [46].

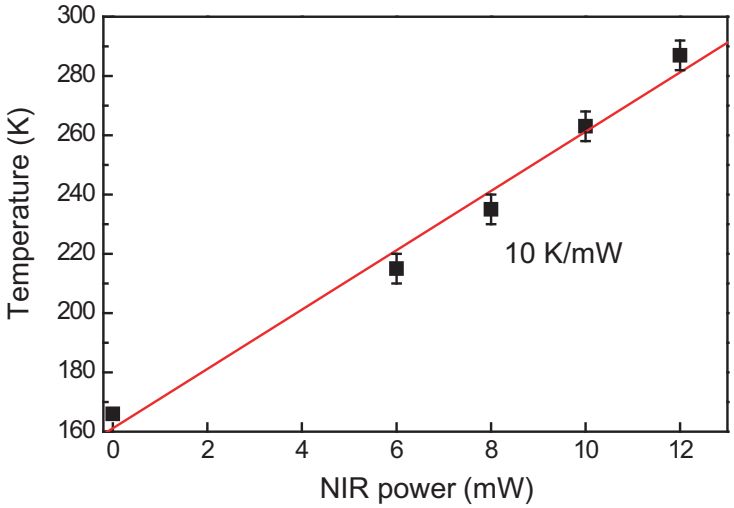

Figure 6.5: Actual temperature calibration with anisotropy in the center of the heating spot as a function of heating power. The temperature scales linearly with applied power with a slope of 10.0 K/mW (solid line). The first data point is given by the cryostat temperature and the accuracy of the calibration is ± 5 K, indicated by error bars.

6.2.4 Data analysis

The FRET efficiency from the fluorescence intensity traces was calculated by means of the following equation:

$$E = \frac{I_A}{I_A + \gamma I_D} \quad ,$$

Where, I_A and I_D are acceptor and donor intensity (after background subtraction and crosstalk correction) respectively, and $\gamma = \frac{\Phi_A \eta_A}{\Phi_D \eta_D}$ is a parameter correcting for the photophysical properties of the dyes. Φ_A and Φ_D are acceptor and donor quantum yield, and η_A and η_D are acceptor and donor detection efficiency respectively. For the optical setup and the fluorophores used in this study, γ is estimated to be close to unity.
A Labview-based analysis routine was used to facilitate automatic FRET calculation from the raw intensity traces recorded with temperature cycles. The analyzing algorithm involves a selection step to take only the signals above a predefined threshold for further calculation in each channel, which sometimes

leads to no FRET value in some cycles if the associated signals are below the threshold.

6.3 Results

In dual-labeled polyproline constructs, Alexa 488 and Alexa 594 were chosen as the FRET pair. These two dyes are frequently used in fluorescence measurements, however there are no detailed studies of their photophysical properties available from literature neither at room-temperature nor at low temperature. Therefore, before we performed the FRET measurements on the full constructs, we first checked the photophysical behavior of the donor from Alexa 488-labeled polyproline10 molecules in glycerol. Figure 6.6 A shows a fluorescence image of this donor-only labeled construct. Most of the bright spots in the image originate from single emitters, as evidenced by a single step bleaching behavior in the relevant fluorescence time traces measured afterwards. Examples of two traces taken from two bright spots in this image are shown in Figure 6.6 B and C, respectively. Both traces show a clear single step bleaching, and additionally trace B has a fluorescence intermittence, the fingerprint of photoblinking, for about 20 s before the molecule is bleached. The blinking events sometimes can be seen in the scanned image as well. For instance, the spot in the middle of the right edge has a clear black stripe in it, indicating a dark state of the fluorophore during raster scanning that line. We also measured single Alexa 594 alone in glycerol at low temperature and the photoblinking was observed as well (data not shown). Here, we did not intend to do systematic photophysical studies of these two dyes. Rather we wanted to have a general impression about their photophysics in glycerol at temperatures below the glass transition (190 K).
We performed static FRET measurements first on dual-labeled polyproline 6 molecules at temperatures below the glass transition of glycerol where the molecules were frozen in the host matrix. Figure 6.7 shows a fluorescence image of this construct recorded at 170 K by exciting the donor. Representative fluorescence time traces from some of these molecules are shown in Figure 6.8. Because of the interplay of the photophysics of the donor and acceptor, the behaviors of their fluorescence time traces were very different from what we expected. In an ideal situation, the two signals from the donor and acceptor should be anticorrelated, i.e., when the acceptor is bleached or in a dark state, the signal from the donor is increased to a new level before it is bleached. This was indeed observed (see trace A after t=50 s and trace D at t=60 s), but very rarely. Frequently, we saw the acceptor intensity was positively correlated with

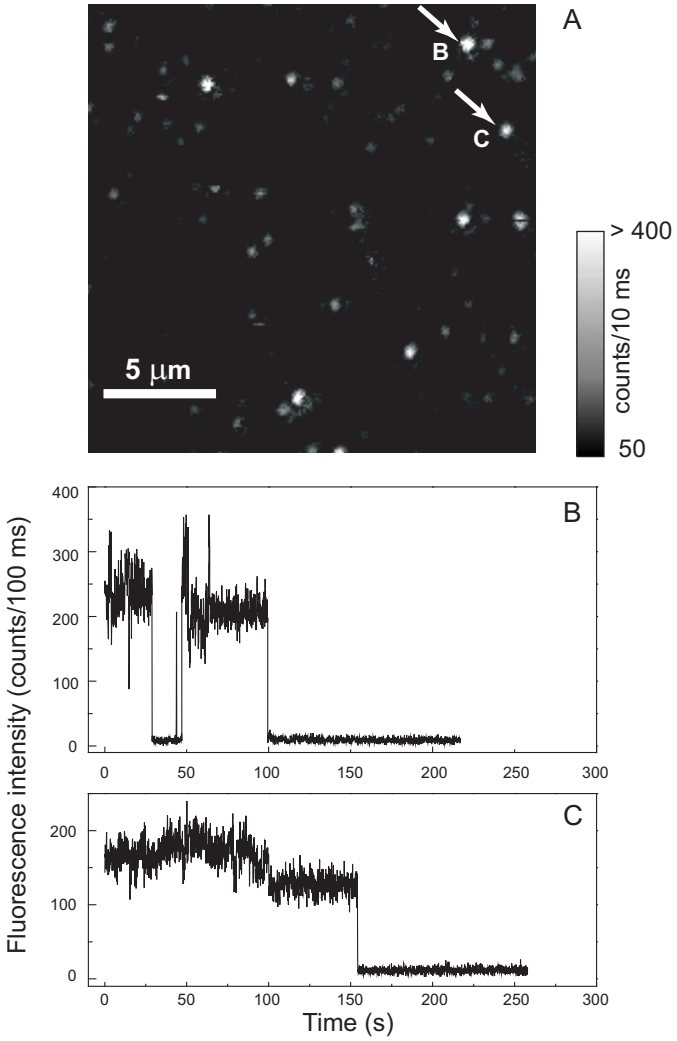

Figure 6.6: A confocally scanned fluorescence image of Alexa 488-labeled polyproline 10 molecules in glycerol recorded at 159 K (A) and examples of fluorescence time traces taken from two bright spots in this image (B & C). (A) The image was scanned by 200×200 pixels, an integration time of 10 ms, and an excitation power of 2.0 kW/cm^2. The scale bar is 5 µm. The two bright spots indicated by the arrows from the image were further analyzed by recording their time traces with a time resolution of 100 ms and an excitation power of 100 W/cm^2, which are shown in (B) and (C), respectively. Both traces show a single-step bleaching behavior, indicating the origin of a single emitter. In addition, there was a dark period of about 20 s in trace B, showing the photoblinking of the fluorophore. Blinking events can also be seen in the image, for example the spot in the middle of the right edge has a clear black stripe in it, indicating a temporary dark state of the fluorophore during raster scanning that line. Most of the bright spots in the image stem from single polyproline constructs.

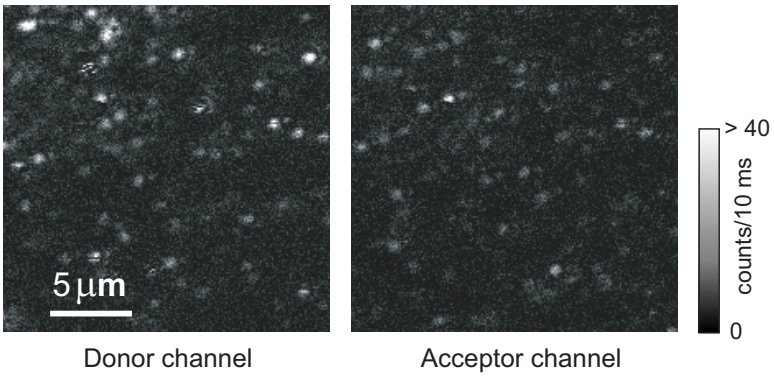

Figure 6.7: A confocally scanned fluorescence image of dual-labeled polyproline 6 molecules in glycerol excited with the 488nm laser at 170 K. The images were scanned by 200×200 pixels, an integration time of 10 ms, and an excitation power of 2.0 kW/cm^2. The bright spots in the acceptor channel indicate the occurrence of FRET.

the donor intensity as shown in trace B and C. This correlated behavior can be explained by the photoblinking and bleaching of the donor, which prevents energy transfer from the donor, hence emission from the acceptor. Sometimes, we observed that a non-fluorescing state of the acceptor did not trigger the increase of the donor signal (see trace D before t=40 s), indicating that this dark state of the acceptor can still accept the excitation energy from the donor. This non-fluorescing quenching could even happen when the acceptor was bleached (see trace E).

The static FRET efficiencies were calculated from the fluorescence time traces of frozen molecules. Figure 6.9 A shows the histogram of the FRET efficiencies of 80 molecules. Instead of the narrow peaked distribution observed at room-temperature [43], our low temperature measurements revealed a very broad distribution spanning the full range of the FRET values. According to the Förster theory, the FRET efficiency, E, depends not only on the interdye distance, R, but also on the relative orientation of the two dyes, κ^2. In first approximation, the dual-labeled polyproline 6 construct can be considered as a short rigid spacer (about 1.8 nm) flanked by a FRET pair of dyes, assuming R is constant. This leaves κ^2 as the only variable for the FRET efficiency. In this approximation, the observed broad distribution of FRET efficiency therefore reflects the distribution of κ^2. If the dye molecules were frozen into various angular configurations randomly at a fixed distance, the distribution of the

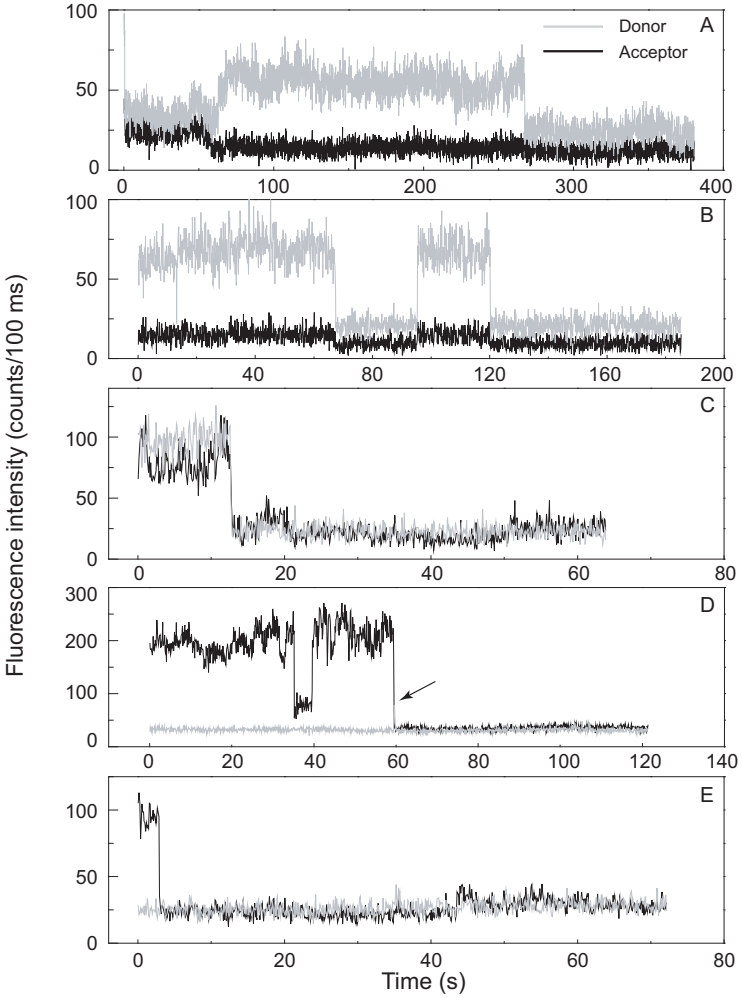

Figure 6.8: Representative fluorescence time traces from frozen dual-labeled polyproline 6 molecules. All the traces were recorded by the donor excitation with an integration time of 100 ms and an excitation power of 1 kW/cm^2 except for trace D 2 kW/cm^2. (A) The two intensities varied in phase in the first 60 s. Then the acceptor intensity went down to the background level and the donor intensity went up to a new level before it was finally bleached. (B & C) The intensities of the donor and acceptor changed in a correlated manner. (D) The donor intensity was on the background level in the first 60 s, whereas the acceptor intensity was relatively high, indicating a high FRET efficiency. However, the acceptor had a period of low emission during which the donor intensity did not recover. When the acceptor was bleached, the donor intensity simultaneously jumped up, indicated by the arrow, but went down to the background level very quickly. (E) The traces showed a high FRET efficiency in the beginning. When the acceptor was bleached, the donor intensity still remained the same.

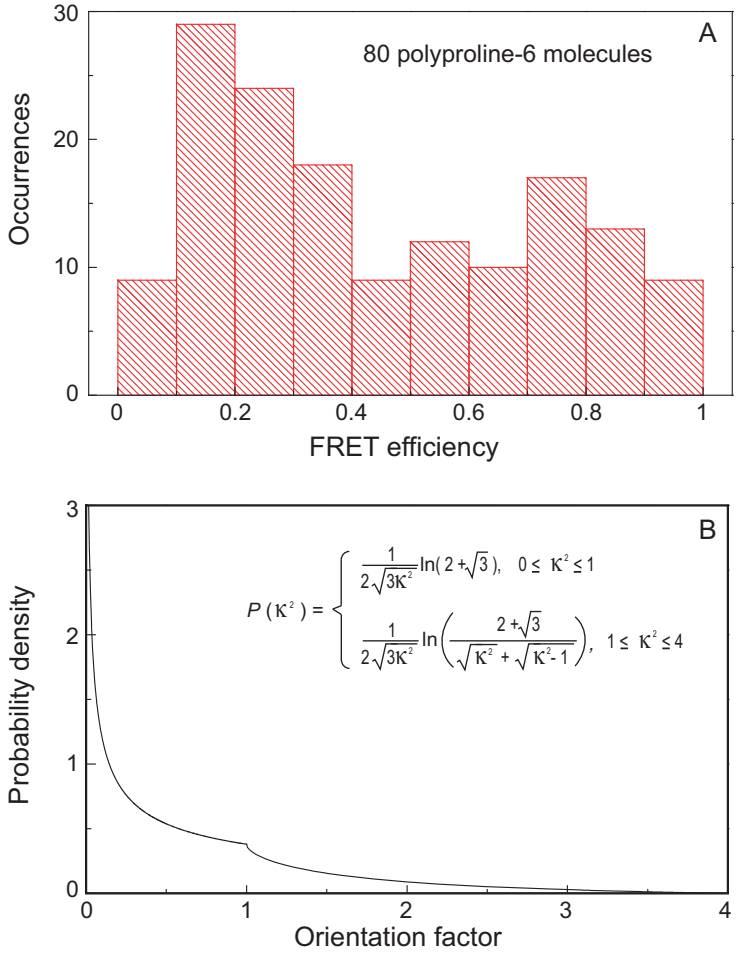

Figure 6.9: Histogram of the FRET efficiencies measured from 80 polyproline 6 molecules (A) and probability density function of κ^2, the orientation factor, for the freely rotating dyes (B).

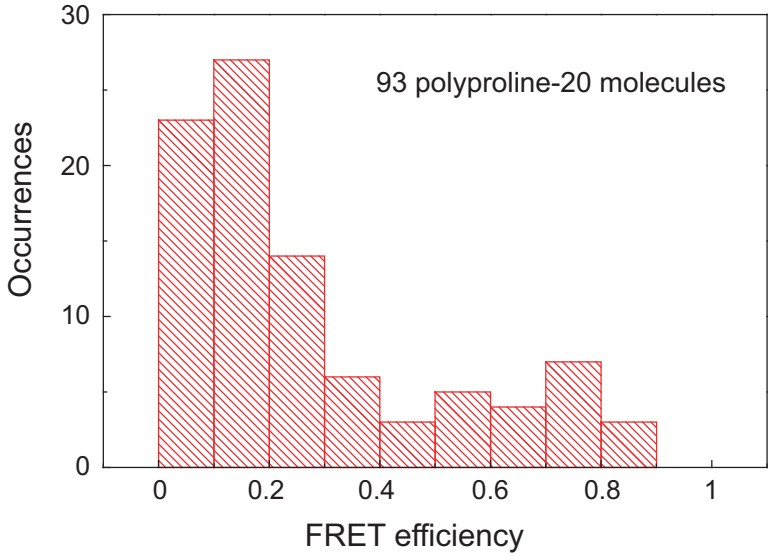

Figure 6.10: Histogram of the FRET efficiencies of 93 polyproline 20 molecules.

FRET efficiency would just follow the probability density function of κ^2 as shown in Figure 6.9 B. According to this probability density function, there is a high probability of identifying a low FRET efficiency and a low chance of finding a high FRET value. The measured FRET distribution is partially consistent with this prediction, i.e., many molecules have low FRET values. However, there are still a number of molecules that have relatively high FRET efficiencies, for example in the peak formed around 0.8 in the histogram. The distribution of the FRET efficiency uncovered from dual-labeled polyproline 6 constructs suggests that the donor and acceptor molecules were not free to sample all the possible orientations. This non-isotropic behavior might be due to the choice of the solvent, glycerol. Since the polyproline 6 molecules were dissolved in this viscous matrix, some configurations may be thermodynamically restricted during slow cooling (5 K/h). Static FRET measurements were also tried on the dual-labeled polyproline 20 construct. They again revealed a broad distribution of the FRET efficiency in which many molecules have FRET values below 0.5, the averaged FRET efficiency measured from the same construct at room-temperature [43], and very few have relatively high values between 0.5 and 0.9 (see Figure 6.10).
We carried out our first temperature-cycle FRET measurements on polyproline 6 molecules. The employed temperature-cycle scheme is shown in Fig-

ure 6.4. In each cycle, we started with exciting the donor only with the probing laser (488 nm) at low temperature for a period of 300 ms during which the FRET from a frozen molecule was probed. A short delay (100 ms) then followed to wait for the full closure of the probing beam. The heating beam was switched on after this delay for a very short time (10 µs) during which the local temperature quickly jumped to a high temperature at which the conformation of the molecule was expected to change. When the heating was off, the molecule was frozen into a new conformation, which would be probed in the next cycle. A second delay was put at the end of the cycle to ensure that the temperature relaxed back to the original low temperature before the next probing began. As mentioned before, for polyproline 6 molecules, the FRET efficiency, in first approximation, can be related to the relative orientations of the two dyes, we therefore expect to see a variation of the FRET efficiency due to reorientations of the donor and acceptor in the temperature-cycle measurements. This indeed can be detected. Figure 6.11 shows two such examples of the fluorescence time traces with temperature cycles recorded at 171 K. Each peak in the traces is a probing event and what is in between is the heating period together with the two delays. With 10 mW heating power, the local temperature is estimated to be around 271 K. Considering the associated viscosity (about 13.6 Pa·s) and the heating period (10 µs), we expect to detect reorientations of the labels, occurring on the time scale of a few microseconds (assuming a hydrodynamic radius of 0.5 nm for the two labels). The rotation time of the whole molecule is about 50 µs at 271 K (assuming a hydrodynamic radius of 1.5 nm for dual-labeled polyproline 6). In panel A, the FRET efficiency probed from the first 11 cycles fluctuated around 0.33 ± 0.1, which might suggest that there were no significant conformational rearrangements within the molecule when it was cycled to a high temperature. However, in the 13th cycle (t=11.5 s), the FRET value suddenly jumped to 0.82 and then went down to 0.73 and 0.61 in the following two cycles. After that, the efficiency went up again to 0.9 and then dropped back to 0.3 before the donor was finally bleached. These consecutive large variations of the FRET efficiency clearly indicate pronounced reorientations of the two labels within the molecule during these temperature cycles. Panel B shows another example in which the molecule with low FRET configurations in the first 30 s suddenly switched to high FRET conformations and persisted for about 63 s before the acceptor was bleached. Thus, fast thermal cycling between a low and high temperatures can induce conformational changes of dual-labeled polyproline 6 molecules, which can be probed by measuring the FRET efficiency.

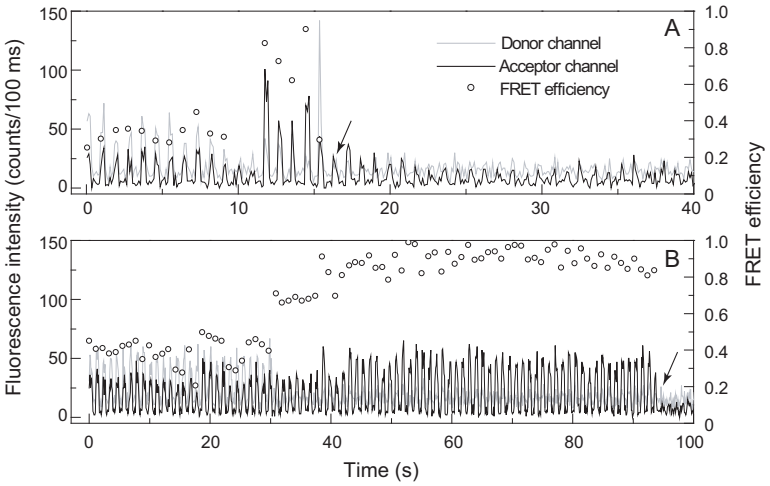

Figure 6.11: Two examples of the fluorescence time traces of polyproline 6 with temperature cycles. The fluorescence time traces were recorded at 171 K with a bin time of 100 ms. In each cycle, the molecule was first excited by the 488 nm laser for 300 ms with a power of 400 W/cm^2. This probing event manifested as a peak in each channel. The associated FRET efficiency (empty circle) was calculated from the two peaks in the donor (gray line) and acceptor (black line) channels, respectively. The molecule was then heated up to a high temperature (about 271 K) by the 785 nm NIR laser for 10 µs with a heating power of 10 mW. The heating event, which was flanked by the two delays (100 ms each), took place between the peaks in the traces. (A) The FRET efficiencies probed in the first 11 cycles fluctuated between 0.25 and 0.45. In the next two cycles, the two signals were very close to the background levels and thus no FRET was calculated according to the selection criteria (see Data analysis in Experimental methods section). In the 13th cycle, the FRET efficiency suddenly increased to 0.82 and went down to 0.73 and 0.61 in the following 2 cycles. It jumped back again to 0.9 in the new cycle and then dropped to 0.3 before the donor was finally bleached (denoted by the arrow). These large consecutive changes of the FRET efficiency clearly indicate pronounced conformational changes within the molecule during these cycles. (B) The molecule began with low FRET configurations (≤ 0.5) and changed to high FRET conformations around $t = 30\,s$. These high FRET conformations lasted for about 63 s before the acceptor was bleached (denoted by the arrow).

6.4 Discussion

We first briefly looked at the photophysics of the donor (from Alexa 488-labeled polyproline 10) and the acceptor (Alexa 594 alone) in glycerol respectively at temperatures below the glass transition. We found that both of them showed photoblinking. This is not very surprising since these two dyes are derivatives of Rhodamine 6G (R6G) and R6G has been shown to have a long-lived dark state in polyvinyl alcohol [96] and glycerol [46] due to formation of a radical ion from the triplet state. The same mechanism might apply to Alexa 488 and Alexa 594 in glycerol as well.

When we recorded the fluorescence time traces from individual dual-labeled polyprolines, we observed three types of relations between the donor and acceptor signals due to the interplay of their photophysics. (1) A correlation between the two signals was often detected, i.e., the acceptor fluorescence intensity was positively correlated with the donor intensity, when the donor molecule was in a dark state or photobleached. (2) A noncorrelation, i.e., the donor intensity remained constant even when the acceptor stopped emitting photons, was frequently seen when the acceptor was in a non-fluorescing state, either a temporary dark or bleached state. This noncorrelated behavior suggests that the non-fluorescing form(s) of Alexa 594 can still quench the emission of Alexa 488. This is probably because the absorption spectrum associated with such non-fluorescing form(s) is very similar to or even identical with that of the fluorescing state of the acceptor although its fluorescence is extinguished. The energy transfer between the two molecules therefore remains more or less the same efficiency. (3) An anticorrelation, which we expected, was found in rare cases. When the acceptor ceased emitting photons, the fluorescence intensity of the donor simultaneously increased to a new level until the donor was finally bleached. This may be due to the blue shifted absorption spectrum of the acceptor after its photobleaching. Since a dark state of the acceptor can lead to a zero FRET efficiency and this should be distinguished from a null FRET resulting from a zero κ^2, one possibility would be to insert another probing event in each temperature cycle to check the photophysical state of the acceptor, as often used in room-temperature single-molecule FRET measurements [139, 140], and the integrity of the constructs, e.g., the presence of constructs without acceptor.

The static FRET measurements on frozen polyproline 6 molecules revealed a broad FRET distribution. This is in big contrast to the narrow peaked distribution observed at room-temperature [43]. The interdye distance ($0.15\,nm < R < 3.45\,nm$) of this construct is rather short and thus high FRET efficiencies are expected from the measurements. However, since the molecules were frozen

in the host matrix, the orientation factor (κ^2), which normally is assumed to be 2/3 in room-temperature FRET measurements, would vary between 0 and 4 if the two dyes were free to rotate. The observed broad FRET distribution therefore partially reflects the distribution of κ^2. However, this distribution is different from the one predicted for an isotropic reorientation of the dyes, suggesting that the motion of the two labels was somehow hindered within the construct. This may be due to the chemical differences between glycerol and water molecules. The water molecule is much smaller and more polar than glycerol, therefore it could easily break possible hydrogen bond(s) formed within the construct, making the labels free to reorient. Such a lubricating role of water molecules has been reported in the studies of rotaxane, a hydrogen bond-assembled synthetic molecular machine [141, 142]. This lubrication might be difficult if the labeled molecules are dissolved in glycerol because the glycerol molecules are rather large, resulting in steric hindrance for disrupting hydrogen bonds. In addition, glycerol molecules themselves can form an extended network of hydrogen bonds, which reduces the mobility of both glycerol and the construct. Therefore, some configurations of the molecules with high free energy, which can form transiently in a normal buffer solution, may be forbidden in glycerol at room-temperature. In addition, more energetically unfavorable configurations will be excluded during the slow cooling (5 K/h). A computer simulation may help us to understand how glycerol influences the dynamics of the polyproline 6 construct. In the future, we would also like to repeat static FRET measurements on this construct in a normal buffer solution, which is more physiologically relevant. Such measurements may uncover a different FRET distribution and more dynamics at a desired high temperature (T_{high}) in temperature cycles. For polyproline 20, we also observed a broad FRET distribution. Although the broadening was also seen in the room-temperature measurements where the well-defined peak was centered around 0.5 in the histogram, our low-temperature measurements showed that most of the molecules have FRET efficiencies below 0.5 and only a few of them have high FRET values between 0.5 and 0.9. This broad FRET distribution again originated from the interplay of the orientation factor ($0 \leq \kappa^2 \leq 4$) and the interdye distance ($4.35\,nm < R < 7.65\,nm$). All the data in these two histograms were taken from the full constructs with non-zero FRET efficiencies. Due to the limitation of the employed detection scheme, populations of full constructs with zero FRET and donor-only constructs may be missing in the histograms. As discussed before, an alternating-laser excitation will be incorporated in our setup to eliminate this limitation [139, 140].

The dynamic FRET measurements on polyproline 6 with temperature cycles

clearly demonstrate that conformational changes of the molecules, which take place at a high temperature, can be probed at low temperature by measuring the FRET efficiency. Due to the limited time available for finishing this thesis, we have not tried to play around with the experimental parameters, such as the heating power and heating period in temperature cycles. The relatively stable FRET efficiencies in Figure 6.11 B indicate that the conformational memory has not been removed completely in glycerol with the applied heating power. Perhaps a higher heating power or replacing glycerol with a normal buffer solution would lead to more detectable dynamics. In addition, to better characterize how the orientation factor influences the FRET efficiency, a well defined model system is needed, for example a double-stranded DNA molecule flanked by two labels with linkers much shorter than the length of the molecule. Even though we only performed few temperature-cycle measurements, we can obtain snapshots of a fast dynamic process of single-molecules with temperature-cycle microscopy. This is not possible with conventional single-molecule spectroscopy at room-temperature. Thus temperature-cycle microscopy will be a new platform on which different probing approaches can be adapted to study fast molecular dynamics at the single-molecule level.

6.5 Conclusion

We studied the conformational dynamics of polyprolines by single-molecule FRET combined with a new type of temperature-cycle microscope developed in our group. We first characterized the static FRET efficiency of individual frozen constructs in a thin glycerol film at low temperature. Both the measurements on polyproline 6 and polyproline 20 revealed a broad FRET distribution. The broadening was ascribed to the interplay of the orientation factor and the interdye distance. Additionally, in the fluorescence time traces of the individual constructs, we saw that the donor and acceptor signals varied in three different manners due to their photophysics. (1) A correlated behavior, i.e., the acceptor intensity was positively correlated with the donor intensity, was detected when the donor was in a dark state or bleached. (2) A noncorrelated behavior, i.e., the change of the acceptor signal was independent of the donor signal, was seen when the acceptor was in non-fluorescing states and it can still accept the excitation energy from the donor. (3) An anticorrelated behavior, i.e., a decrease in the acceptor intensity was coupled to an increase of the donor intensity, was observed if a non-fluorescing form of the acceptor was not able to quench the donor emission. We performed our first temperature-cycle measurements on polyproline 6 molecules and we could indeed detect the con-

formational changes of the individual molecules induced by temperature jumps by following the variation of the FRET efficiency. These preliminary results show that our proposed temperature-cycle microscopy combined with single-molecule FRET labeling has potential for studies of protein-folding dynamics at the single-molecule level.

Acknowledgements

We thank Prof. Benjamin Schuler for kindly providing us with dual-labeled polyproline samples.